Surface complexation modeling of Cd(II) sorption to montmorillonite, bacteria, and their composite

Ning Wang[1,2]*, Huihui Du[1,2]*, Qiaoyun Huang[1,2], Peng Cai [1,2], Xingmin Rong[2] and Wenli Chen[1,]****

[1] State Key Laboratory of Agricultural Microbiology, Huazhong Agricultural University, Wuhan 430070, China.

[2] Key Laboratory of Arable Land Conservation (Middle and Lower Reaches of Yangtze River), Ministry of Agriculture, College of Resources and Environment, Huazhong Agricultural University, Wuhan 430070, China.

*These authors contributed equally to this work.

**Corresponding author: Q. Huang, E-mail: qyhuang@mail.hzau.edu.cn; W. Chen, wlchen@mail.hzau.edu.cn; Tel: +86-27-87671033; Fax: +86-27-87280670

Abstract

Surface complexation modeling (SCM) has emerged as a powerful tool for simulating heavy metal adsorption processes on the surface of soil solid components under different geochemical conditions. The component additivity (CA) approach is one of the strategies that have been widely used in multi-component systems. In this study, potentiometric titration, isothermal adsorption, zeta potential measurement, and extended X-ray absorption fine structure (EXAFS) spectra analysis were conducted to investigate Cd adsorption on 2:1 clay mineral montmorillonite, on Gram-positive bacteria *Bacillus subtilis*, and their mineral-organic composite. We developed constant capacitance models (CCM) of Cd adsorption on montmorillonite, bacterial cells, and mineral-organic composite. The adsorption behavior of Cd on the surface of the composite was well explained by CA-SCM. Some deviations were observed from the model simulations at pH < 5, where the values predicted by the model were lower than the experimental results. The Cd complexes of X_2Cd, $SOCd^+$, $R\text{-}COOCd^+$, and $R\text{-}POCd^+$ were the predominant species on the composite surface over the pH range of 3 to 8. The distribution ratio of the adsorbed Cd between montmorillonite and bacterial fractions in the composite as predicted by CA-SCM closely coincided with the estimated value of EXAFS at pH 6. The model could be useful for the prediction of heavy metals distribution at the interface of multicomponents and their risk evaluation in soils and associated environments.

Keywords: montmorillonite, bacteria, composite, Cd(II), sorption, modeling

1. Introduction

Anthropogenic activity and industrialization release large quantities of heavy metals into soils (Fomina and Gadd, 2014; He and Chen, 2014). The interactions between soil solid components and heavy metals in complex natural systems should be understood in order to predict their transport and fate. Surface complexation modeling (SCM) is a powerful tool for describing adsorption processes and mechanisms under different geochemical conditions (Dong and Wan, 2014; Wang and Giammar, 2013). SCM has been adopted to simulate the adsorption of heavy metals on the surface of soil solid components such as kaolinite (Angove et al., 1997), montmorillonite (Akafia et al., 2011; Benedicto et al., 2014; Bradbury et al., 2005; Ikhsan et al., 2005; Soltermann et al., 2014), magnetite (Kim et al., 2012), manganese oxide (Wang et al., 2013), fulvic and humic acid (Christl et al., 2001; Koopal et al., 2005; Milne et al., 2003), natural organic matter (Koopal et al., 2005; Gustafsson et al., 2014), and bacteria (Borrok and Fein, 2005; Borrok et al., 2004; Daughney et al., 2001; Fein et al., 2001; Kenney and Fein, 2011; Liu et al., 2013; Moon and Peacock, 2011).

Soil solid components, which include bacteria and clay minerals, often exist as composites in natural environments. The component additivity (CA) approach has been widely used in the application of surface complexation models for describing heavy metal adsorption on mixtures and on the composites of soil solid components. The component additivity-diffuse layer model (CA-DLM) has been successfully applied to model the adsorption of Co^{2+} (Landry et al., 2009), Cd^{2+} (Reich et al., 2010),

and Pb^{2+} (Reich et al., 2010), on mixtures of hydrous ferric oxide (HFO) and quartz with kaolinite. Dong and Wan (2014) indicated that the CA-SCM can provide excellent predictions for uranium (VI) adsorption on quartz-sand dominated sediments. Fowle and Fein (1999) concluded that the CA approach can be used to model the adsorption of Ca^{2+}, Cu^{2+}, Cd^{2+}, and Pb^{2+} on mixtures of *Bacillus licheniformis* and *B. subtilis*. Additionally, CA could successfully describe Cd, Co, Sr, and Zn adsorption onto the mixtures of 10 species of Gram-positive bacteria (Yee and Fein, 2001). For the mixtures of minerals and organic systems, the extended constant capacitance model was used to depict Cd^{2+} adsorption onto goethite, kaolinite, and muloorina illite in the presence of citric acid (Lackovic et al., 2004a,b). The linear additivity model has succeeded in predicting Cu^{2+} adsorption, but has failed to simulate Ca^{2+} adsorption on goethite in the presence of fulvic acid (Weng et al., 2008). The adsorption of Cd^{2+} onto *Comamonas spp.*–ferrihydrite composite could be accurately predicted by the addition of the reaction between end-member ferrihydrite and bacteria (Song et al., 2009). However, the amount of Cd^{2+} adsorption onto the composite was up to 10% lower than that predicted by the additive approach. In the study of Alessi and Fein (2010) the CA approach was applied to describe the extent of Cd adsorption on the surface of two- and three-component mixtures of *B. subtilis* cells, HFO, and kaolinite at various mass ratios in the presence of acetate. The models matched well with experimental data in the absence of acetate, whereas they underestimated Cd adsorption in the presence of acetate. Moon and Peacock (2013)

found that Cu adsorption behavior on ferrihydrite–*B. subtilis* composites with ferrihydrite as the major component can be modeled by a component additivity approach. By contrast, composites with a majority of bacteria component cannot be simulated by a component additivity approach, and significant deviations were observed.

Previous studies concerning surface complexation models have mainly focused on heavy metal adsorption by individual minerals or bacteria or mineral–organics and metal oxide–bacteria composites. To the authors' knowledge, no SCM investigation using 2:1 clay mineral–bacteria composites, has been performed. Montmorillonite, a representative of the 2:1 phyllosilicates, exhibits large specific surface area and high cation exchange capacity, which make it an effective adsorbent for heavy metals. The clay mineral is widely distributed in a variety of soils in temperate zone. The model developed in clay mineral–bacteria composites will provide insights into the behaviors of heavy metals in contaminated soils of these regions. Thus, in this study, we first develop surface complexation models for Cd adsorption on end-member 2:1 clay mineral montmorillonite, Gram-positive bacteria *Bacillus subtilis*, and finally their mineral-organic composite by using the component additivity (CA) approach. Moreover, linear combination fitting of the extended X-ray absorption fine structure (EXAFS) spectra were applied to verify the distribution ratio of Cd between different components derived from CA-SCM.

2. Materials and Methods

2.1. Adsorbent and Reagent

Montmorillonite, (Sanding Group Co. Ltd., Shaoxing, Zhejiang, China), was prepared following previously outlined procedures (Hong et al., 2012; 2013). The clays were oxidized using H_2O_2 (30%) to remove any residual organic matters. The < 2 μm colloidal fractions were isolated through sedimentation. The specific surface area, determined by the BET method (N_2 adsorption), was found to be 60.2 m^2 g^{-1}. Previous study showed that a particle was estimated to be formed of nearly 20 stacked layers in the dehydrated state used in the gas adsorption experiment (BET' method), whereas it was estimated to be composed of only 1 or 2 layers in aqueous suspension (Tournassat et al., 2003). Thus, the values derived from BET' method usually underestimate the actual total surface area in aqueous. Herein, we set the SSA of montmorillonite to be 800 m^2 g^{-1}, and the detailed processing procedures are shown in Supporting Information.

The test bacteria used in this study came from the aerobic Gram-positive species *B. subtilis*, which were obtained from the State Key Laboratory of Agricultural Microbiology. The microorganisms were inoculated into 10 mL LB medium and cultured for 7 h at 28 ℃ to reach the exponential phase with an optical density of 1.4 at 600 nm (OD600 nm). Subsequently, 2 mL of the resulting bacterial suspension was transferred to 200 mL LB medium for another 18 h inoculation (OD_{600nm}=2.7) to reach the mid-exponential phase. Cells were pelleted by centrifugation at approximately 7200 *g* for 5 min and rinsed three times in ultrapure water. The ratio of

137 the wet weight to dry (60 ℃ in drying oven) weight of the biomass is 9:1. The
138 biomass mentioned in this paper all refer to dry weight.

139 Montmorillonite and the bacterial cells were suspended in 0.01 M $NaNO_3$ to
140 produce the suspensions that were used in the experiments. The
141 montmorillonite–bacteria composite was prepared following a montmorillonite: *B.*
142 *subtilis* mass ratio of 7:1 to produce suspensions (4 h, 28 ℃). The resultant
143 montmorillonite–bacteria composite suspensions were used for subsequent
144 experiments. Preliminary isothermal adsorption (pH 8) of bacteria to montmorillonite
145 results showed that the maximum adsorption predicted by Langmuir equation was
146 approximately 0.14 g (dry cell)/ g (clay) which was equal to a mass ratio (clay to
147 bacteria) of 7:1 (Supporting Information, Fig. S1). Clearly adsorption of bacteria on
148 montmorillonite decreased with the increase of pH, thus bacteria can be completely
149 adsorbed by montmorillonite to a large extent in all experimental conditions (pH
150 3–8.5) at this ratio. The bacterial cells were remain intact under the experimental
151 condition (see AFM images of the Supporting Information, Fig. S2).

152 Analytical reagent grade chemicals were used throughout the study. $Cd(NO_3)_2$
153 was used to prepare 178.0 μmol L^{-1} Cd(II) stock solution. Water was Milli-Q reagent
154 grade.

155

156 **2.2. Zeta potential analysis**

157 Zeta potential analysis was conducted to study the surface charge properties of
158 montmorillonite, *B. subtilis*, and montmorillonite–*B. subtilis* composite. Suspensions

were prepared the same as section 2.1, over the pH range of 3 to 8. Samples were injected into a zeta potential analyzer (Zetaplus90, Brookhaven), and measured in triplicate.

2.3. Potentiometric titrations

Titration experiments were performed (in duplicate) according to the procedures described by Fein et al. (2005). The suspensions (1 g L^{-1}, 40 mL) of montmorillonite and *B. subtilis* and the composite in 0.01 M $NaNO_3$ were placed in a sealed titration vessel maintained under a positive pressure of N_2. Titrations were conducted using an automatic potentiometric titrator (Metrohm titrator 836, Switzerland). Each suspension was first titrated to pH 3 by using 0.1136M HNO_3 solutions and then to pH 8.5 by using 0.0976 M NaOH. At each titration step, a stability of 0.01 mV S^{-1} was attained before adding the next drop of the titrant.

Gran plot was adopted to determine the specific volume of titrant added at the equivalence point (*Ve*) and to derive the total H^+ concentration (TOTH) (Chu et al., 2002; Du et al., 1997; Liu et al., 1999; Liu et al., 2013).

The values for the Gran function (G) were calculated as follows:

$$\text{On the acidic side: } G_a = (V_0 + V_{at} + V_b) \times 10^{-pH} \times 100$$

$$\text{On the alkaline side: } G_b = (V_0 + V_{at} + V_b) \times 10^{-(13.8-pH)} \times 100$$

Gran plots for titration data on montmorillonite and *B. subtilis* are illustrated in Fig. S3, where V_0 stands for the initial volume of the titrimetric suspension; and V_a and V_b represent the total volume of acid and alkaline solution added at each titration point, respectively. In the Gran plots, the OH^- added to a suspension firstly neutralizes

the excess H^+ before V_{eb1}, then reacts with the functional group on the surface of the sorbent between V_{eb1} and V_{eb2}, finally changes the pH after V_{eb2}. No apparent surface reactions consuming OH^- before V_{eb1} were noted. The total concentration of reacting H^+ at each titration point (TOTH) was calculated using the following equation, where C_b stands for NaOH concentration:

$$TOTH = \frac{-(V_b - V_{eb1}) \times C_b}{V_0 + V_{at} + V_b} \quad (\text{mol } L^{-1}),$$

2.4. Adsorption experiment

The adsorption edge experiments were conducted in 0.01 M $NaNO_3$ solutions to investigate the adsorption of Cd onto montmorillonite, *B. subtilis* and the composite. 15 mL 178.0 μmol L^{-1} Cd(II) solution and 15 mL 2 g L^{-1} adsorbent suspensions were added to 50 mL centrifuge tubes. A suitable volume of concentrated HNO_3 or NaOH solutions was added to adjust the pH of the suspensions from 3 to 8. The final concentration of Cd and adsorbents were 89.0 μmol L^{-1} and 1 g L^{-1}, respectively. Fixed pH isotherm experiments were performed at pH 6 and 8 in 0.01 M $NaNO_3$ electrolyte. The initial concentrations of Cd ranged from 8.9–89.0 μmol L^{-1} with a sorbent concentration of 1 g L^{-1}. The mixtures were allowed to equilibrate for two hours at 28 ℃. After equilibration, the final suspensions were centrifuged at 12557 g for 5 min, and the clear supernate was analyzed using atomic adsorption spectroscopy (AAS; Varin AAS240FS) to determine the residue Cd.

Solution speciation of 89.0 μmol L^{-1} Cd(II) in 0.01M $NaNO_3$ was calculated as a function of pH using the geochemical software Visual MINTEQ 3.1. Cd^{2+} was

determined to be the main species at the experimental conditions. $Cd(OH)_2$, $CdOH^+$, and Cd_2OH^{3+} were also found at pH > 7.8, but in relatively small percentages.

2.5. X-ray absorption spectroscopy

We selected pH 6 sample of the adsorption edge experiments in section 2.5 as representative to perform the XAS experiments. The solid phases after centrifugation were transformed immediately to collect XAS spectra in 12 h. The sample holders were packed together with moist tissues (stored at ~ -4^o C) to minimize sample drying during shipment to the Shanghai Synchrotron Radiation Facility (SSRF), China. The X-ray absorption data at the Cd *K*-edge (~26700 keV) of the samples were recorded at room temperature in the fluorescent mode with silicon drift fluorescence detector. The station was operated with a Si(III) double crystal monochromator. During the measurement, the synchrotron was operated at energy of 3.5 GeV and a current between 150–210 mA. EXAFS spectra were collected from 26511 to 27551 eV. Background subtraction and normalization of the XAS data were conducted in ATHENA, a program in the IFEFFIT package (Ravel and Newville, 2005). The background subtraction was performed using PySpline. The pre-edge was fit to a linear function and the post-edge background to two 2nd-order polynomial segments. To obtain information on the partitioning of Cd between the different fractions of the composites, the spectra were fitted using a linear combination fitting procedure (LCF). Cd-adsorbed montmorillonite, Cd-bacteria were used as end-member for the 2-component fitting of the binary composites, with linear combination performed over the k^3-range of 2.3-10 Å^{-1} (force weight to sum to 1). The goodness of the fitting was

224 evaluated by the best-fit criterion values (*R*) (Du et al., 2016).

225 **2.6. Surface complexation modeling**

226 The program FITEQL 4.0 was utilized to determine functional group site
227 concentrations, proton, and metal binding stability constants (Herbelin and Westall,
228 1999). A constant capacitance model was implemented (Tertre et al., 2006). The
229 activity coefficient correction was made within FITEQL using the Davies equation.
230 An indicator of the goodness of the fitting is the overall variance, V, in Y (Herbelin
231 and Westall, 1999). $V_Y = \frac{WSOS}{DF}$, where WSOS is the weighted sum of squares of
232 the residuals and DF is the degrees of freedom. Lower V_Y values signify better fits.
233 The systematic process of developing the SCM was started by fitting the model to the
234 experimental data for montmorillonite and *B. subtilis*.

235 The potentiometric titration data was fit to generate the acid-base constants and
236 surface site densities (Fig. S4). Acid-base reactions on the surface of montmorillonite
237 are represented by the following equations:

238 $SOH \Leftrightarrow SO^- + H^+$ (1)

239 $SOH + H^+ \Leftrightarrow SOH_2^+$ (2)

240 $WOH \Leftrightarrow WO^- + H^+$ (3)

241 $X^- + H^+ \Leftrightarrow XH$ (4)

242 $X^- + Na^+ \Leftrightarrow XNa$ (5)

243 where SOH and WOH are aluminol and silanol sites on the surface of
244 montmorillonite, respectively. X^- is the negative exchange site that can react with both
245 H^+ and Na^+. The total concentration of exchange site and the binding stability

constants of XH, XNa were used as fixed input parameters when the titration data were fitted. These three values were 8.7×10^{-4} mol g^{-1}, -2.2 and 1.4, respectively (Table S1), which come from Tertre et al. (2006) and Soltermann et al. (2014). The acid-base constant and the site density of SOH and WOH were set as iterated parameters, in addition, these parameters were iterated simultaneously.

The acid-base reactions on the surface of *B. subtilis* were represented by

$$R\text{-}L_iH^0 \Leftrightarrow R\text{-}L_i^- + H^+ \quad (6)$$

where R represents the bacterium to which each functional group is attached. Carboxyl sites, phosphate sites, and hydroxyl sites were considered to be the main functional groups on the surface of *B. subtilis* (Yee and Fein, 2001). L_iH^0 represents these three groups.

Acid-base equilibrium constants and site densities (Tables S1 and S2) were used as fixed input parameters in the modeling of the Cd pH adsorption edge and fixed pH isotherm data. The constants of Cd complexes with the functional groups on each sorbent were iterated simultaneously. The following equilibria were used to describe Cd(II) adsorption onto montmorillonite:

$$2X^- + Cd^{2+} \Leftrightarrow X_2Cd \quad (7)$$

$$SOH + Cd^{2+} \Leftrightarrow SOCd^+ + H^+ \quad (8)$$

Due to their higher pK_a, hydroxyl sites are not deprotonated over the range of pH 3 to 8. To simplify the model, hydroxyl sites were not invoked. Cd(II) adsorption on *B. subtilis* was described with the following reaction equilibria:

$$R\text{-}COO^- + Cd^{2+} \Leftrightarrow R\text{-}COOCd^+ \quad (9)$$

$$R\text{-}PO^- + Cd^{2+} \Leftrightarrow R\text{-}POCd^+ \quad (10)$$

Finally, we combined the model of Cd(II) adsorption on montmorillonite and *B. subtilis* to simulate the adsorption behavior of Cd(II) on the composite. End-number montmorillonite and *B. subtilis* models were combined in FITEQL 4.0 using the CA approach.

3. Results

3.1. Zeta potential

The zeta potential of montmorillonite, *B. subtilis*, and montmorillonite–*B. subtilis* composite are given in Fig. 1. Over the whole pH range studied, both montmorillonite and the composite had negative surface charge with very low pH_{pzc} around pH 3.1. The bacteria displayed a negative surface charge at pH > 3.5 and had a higher pH_{pzc} than the value reported by Fein et al. (2005) (pH_{pzc} < 2). The negative electrokinetic charge of all sorbents increased with pH and remained constant when pH was higher than 5. The zeta potential of montmorillonite and bacteria were -2.29 mV and 12.27 mV at pH 3, -26.70 mV and -19.46 mV at pH 8. The surface of the montmorillonite–bacteria composite was more negatively charged than that of montmorillonite and *B. subtilis* at pH > 5, the zeta potential of the composite was -20.30 mV at pH 3.

3.2. Cadmium adsorption

Figure 2 shows the pH dependence of Cd adsorption on montmorillonite, *B. subtilis*, and montmorillonite–*B. subtilis* composite. Adsorption onto montmorillonite increased slowly over the pH ranges, and about 55% of the total Cd(II) was adsorbed at pH 8. Adsorption onto *B. subtilis* increased sharply between pH 3 and 7 and then reached a plateau at pH 7–8. Nearly 90% of total Cd(II) was adsorbed at pH 8. In comparison to bacteria, the uptake of Cd on montmorillonite–*B. subtilis* composite increased more slightly over the range of pH 3 to 8. The extent of adsorption onto the composite increased swiftly from pH 3 to 5, and varied slightly at pH 5–8. About 60% of the total Cd(II) ions were adsorbed onto the composite at pH 8.

3.3. Modeling of Cd adsorption onto montmorillonite and *B. subtilis*

The titration data for montmorillonite and *B. subtilis* are presented in Fig. S4. Bacteria exhibited significant buffering capacity over the range of pH 3 to 8.5, which was assigned to the deprotonation of functional groups on cell walls (Borrok et al., 2004; Moon and Peacock, 2011; Yee and Fein, 2001). Montmorillonite presented strong buffering capacity only at pH < 4 and pH > 7.5. This result was in line with the report of Ikhsan et al. (2005), which also showed similar buffering behaviors of a Ca-montmorillonite over these pH ranges. The titration data of montmorillonite and *B. subtilis* were successfully modeled with reactions (1)–(5) and (6). The protonation constants and site densities of sorbents calculated from titration data are indicated in Tables S1 and S2.

Adsorption of Cd onto the surface of montmorillonite and *B. subtilis* were successfully modeled with reactions (7)–(10). The best-fit for cadmium adsorption on

montmorillonite is depicted in Fig. S5 (a). The adsorption of Cd(II) onto montmorillonite was modeled using two adsorbed species, X_2Cd and $SOCd^+$. The calculated complex stability constants of these two species were 8.30 and -1.68, respectively (Table S1). The complexation of Cd(II) onto two X^- sites (X_2Cd) dominated at pH < 4.5 while monodentate complexation onto SOH sites of the crystal edges ($SOCd^+$) predominated at pH > 4.5. The V_Y value of the model which describes the Cd adsorption on montmorillonite was 5.6. The best-fit model for the Cd adsorption onto *B. subtilis* is presented in Fig. S5 (b). The optimized $logK_{R\text{-}COOCd+}$ and $logK_{RPOCd+}$ values were 2.54 and 2.87, respectively (Table S2). Surface complexation model successfully simulated the adsorption edge of *B. subtilis* over the pH ranges of 3 to 8. The model predicted that one inner-sphere monodentate complexation ($R\text{-}COOCd^+$) dominated at low pH while another inner-sphere monodentate complexation ($R\text{-}POCd^+$) dominated at high pH. The V_Y value of the model which described the Cd adsorption on bacteria was 3.8.

3.4. Modeling of Cd adsorption onto montmorillonite–*B. subtilis* composite

The parameters for the model of Cd adsorption onto montmorillonite–*B. subtilis* composite are shown in Table 1. As per the CA approach, the constants for protonation and the acid-base reactions on the surface of the composite were the same as those for the end-member montmorillonite and *B. subtilis*. The operational site densities of functional groups used in the model of Cd sorption on the composite were calculated based on the end-member site densities weighted to the montmorillonite:bacteria mass ratio (Moon and Peacock, 2013). The specific

capacitance and surface area were calculated in the same way. Four Cd complexation species were considered in the model of Cd sorption on the composite, i.e., X_2Cd and $SOCd^+$ on montmorillonite; two inner-sphere complexes on bacteria. The complexation constants of the four species were the same as those optimized by the models of Cd adsorption on montmorillonite and *B. subtilis*.

The adsorption behavior of Cd on montmorillonite–*B. subtilis* composite was well described by CA-SCM, except some deviations were observed at pH < 5 (Fig. 3, V_Y=15.4). The complex X_2Cd dominated below pH 4. At pH 4.5, the $SOCd^+$ was the major species with deprotonation of the SOH surface sites. At pH 3–5.5, the inner-sphere complex R-$COOCd^+$ on the surface of bacteria contributed 10–20% of the total Cd adsorption. At pH above 5.5, the inner-sphere complex on the bacterial surface (R-$POCd^+$) played an important role and amounted to 10–20% of the total Cd adsorption. The CA-SCM provided an adequate fit to the adsorption isotherms of Cd on the composite at pH 6 and pH 8, with V_Y values of 4.3 and 2.4, respectively (Fig. S6). Figure 4 depicts the distribution of the total adsorbed Cd between the composite fractions. Montmorillonite played a dominating role in Cd sorption on the composite over the whole pH range studied. The percentage for the adsorption of Cd on montmorillonite and *B. subtilis* in the composite at pH 6 was 71.4% and 28.6%, respectively. The V_Y value ranging from 0.1 to 20 can generally be considered a good fit. Overall, within the constructs of FITEQL SCM, CA-SCM is adequate to describe the Cd adsorption behavior on the surface of the composite.

3.5. Distribution of Cd on montmorillonite–*B. subtilis* composite by XAS.

Since the model successfully described Cd adsorption on bacteria-clay composite at pH > 5, herein we selected pH 6 samples to investigate whether model predictions match well with the EXAFS prediction. Linear combination fitting (LCF) procedure has been successfully applied to obtain the partitioning of metal adsorption on bacteria-mineral composites (Du et al., 2016; Moon and Peacock, 2012; Templeton et al., 2003). This approach is based on the intermediate adsorption behavior of metals between the end-member component. The Cd K-edge (EXAFS) spectra of montmorillonite, *Bacillus subtilis* and their composite are shown in Fig. 5. A few differences between the spectrum of mineral and bacteria are pronounced at *k*-values of 6-10 $Å^{-1}$. We were able to produce excellent fits to the Cd-composite spectra with a linear combination of Cd-adsorbed montmorillonite and Cd-adsorbed *B. subtilis* clusters (*R*-factor < 0.1). Linear combination results for the distribution of total adsorbed Cd by the composite yielded a ratio of 69.1%:30.9% for montmorillonite and bacterial cells, respectively. This ratio closely approaches the value obtained from model speculation, which is 71.4%:28.6%.

4. Discussions

A number of investigators have employed CA-SCM to describe metal adsorption onto mineral–bacteria composites (Alessi and Fein, 2010; Moon and Peacock, 2013; Song et al., 2009;). However, to the authors' knowledge, this is the first information on the modelling of Cd adsorption by 2:1 clay mineral–bacteria composites. The species and

distribution of Cd on the surface of montmorillonite–*B. subtilis* composite were modeled using CA-SCM in this study. Cadmium was found to be adequately described by adsorption to the nominally assigned RCOOH and POH sites, and the X^- and SOH groups on the surface of montmorillonite–*B. subtilis* composite. Our results imply that all these groups have to be considered for a successful simulation of Cd adsorption on 2:1 clay mineral-bacteria mixtures, compared to ferrihydrite-bacteria composites where, of the bacterial component, only carboxyl (RCOOH) groups were found to be responsible for heavy metal adsorption over the entire pH range studied (Moon and Peacock, 2013). The model of Cd adsorption on montmorillonite–*B.* subtilis composite in our study suggested that X_2Cd was the major species on the composite at pH < 4. Interestingly, montmorillonite played a dominant role in Cd sorption on the composite (the mass ratio of montmorillonite to bacteria was 87.5%:12.5%) over the entire pH range studied. However, the contribution to Cu adsorption from the components of a ferrihydrite–bacteria mixture with a mass ratio of 82%:18% was dependent on pH (Moon and Peacock, 2013). Bacteria and ferrihydrite governed Cu adsorption at low and high pH values, respectively. The montmorillonite has a permanently charged XH site, which provides a certain level of adsorption capacity independent of pH, whereas the ferrihydrite-bacteria composites to which the authors are contrasting their work possess only amphoteric sites (Moon and Peacock, 2013). Our data revealed that the percentage of total adsorbed Cd on montmorillonite in the composite was in the range of 87.3–69.1% from pH 3 to 8

(Figure S7). These results suggest that the bacteria fraction in the composite plays an increasingly important role in the retention of cadmium ions from pH 3 to 8, although slight decreases in Cd attachment were observed for the bacteria from pH 4 to 5. Some of the Cd ions may have been transferred from the montmorillonite surface to the bacteria in the composite with the rise of pH.

The modelled distribution of Cd on individual components in our montmorillonite–*B. subtilis* composite was supported by the EXAFS investigations at pH 6. The ratio of Cd adsorption onto montmorillonite to that of the bacterial cells present in the composite as obtained from EXAFS spectra analysis closely coincides with the value obtained from model speculation. Both the model simulation and EXAFS observation from our study suggested that the fate of Cd is largely affected by the presence of montmorillonite in soils and sediments, particularly in locations where the mineral exists as the major clay mineral component. Our 2:1 clay–bacteria system is different from the 1:1 clay–bacteria system reported by Alessi and Fein (2010), where they found that the majority of Cd is predicted to occur onto the permanent structural site of the kaolinite component only below pH 4 in a kaolinite–*B. subtilis* mixture dominated by the mineral fraction (75%), and *B. subtilis* contribute nearly 58% of the total reactive site. Templeton et al. (2003) reported that 71% and 29% of Pb ions were adsorbed by goethite and bacteria in a goethite–bacteria composite with a mass ratio of 70% : 30% at pH 7. Moon and Peacock (2012) found that the distribution of Cu adsorption between ferrihydrite and bacteria fractions in a

ferrihydrite–bacteria composite (with a mass ratio 65% : 35%) was 80% : 20% at pH 6.4. Our work thus corroborates the findings of Moon and Peacock (2012) who predict that, in mineral-organic composites dominated by the mineral component, the mineral will be responsible for the majority of the heavy metal adsorption and the composites will behave approximately additively. Moreover, this study has extended their work which was based on iron (hydr)oxide-organic composites, to clay mineral-organic composites. The established models from these investigations may provide a universal rule to predict the behavior of trace metals in more complicated ecosystems bearing mineral–organic complexes.

Our study provides useful insights on clay-bacteria interactions in the biogeochemical interface of complex soil and its environmental consequence. Although surface complexation modeling (SCM) has been widely applied to describe trace metal adsorption behaviors on various soil solid components, how to apply it in complex systems is still challenging. The present results indicate that Cd adsorption behaviors on montmorillonite-bacteria composite is successfully described by CA-SCM model, except for some deviations at pH < 5. Current SCM models might be useful for the prediction of the distribution of Cd between solid and solution phases in a variety of settings. Soils and various sediments are composed of clay minerals, organic matter and microorganisms. It is critical to model Cd adsorption and availability at the interface of multi-components interactions which is fundamental for the risk evaluation of Cd-contaminated environments, especially those in temperate

regions such as brown clay and black clay soils which are dominated by 2:1 clays. Secondly, the fact that the distribution of Cd between the end-member component is dependent on pH, has important implication for Cd mobility. The adsorbed Cd complexes, either outer-sphere or inner-sphere, may exhibit different exchange or desorption behaviors during the changes of environmental factors, e.g., cations, redox potential. The relative mobility of clay– and organic –adsorbed Cd might differ. Under this premise, mineral-organic composite is a suitable analogue for a good predictor of the mobility and thus eventual fate of Cd in natural environments. Lastly, our study has implications for the remediation of Cd contaminant soils and sediments where 2:1 phyllosilicates dominate the mineral composition, in particular, when various organic agents are applied, e.g., straw, manure or engineering microorganisms. These substances are easily bound to soil mineral surface. In these cases, it is vital to consider the fate, mobility of heavy metals with respect to mineral-organic composites, in addition to pure mineral phases.

5. Conclusions

In this study, we developed surface complexation model for Cd(II) adsorption on montmorillonite, *B. subtilis*, and their composite. The Cd adsorption behavior onto the surface of the composite can be described by a component additivity approach (CA-SCM). Underestimation was observed for the model prediction at pH < 5. The X_2Cd, $SOCd^+$, $R\text{-}COOCd^+$, and $R\text{-}POCd^+$ were the predominant species of Cd adsorbed on the surface of montmorillonite–*B. subtilis* composite. Montmorillonite

played a more important role for the binding of Cd ions in the mineral–bacteria composite over the ranges of pH 3 to 8. The distribution of adsorbed Cd between the montmorillonite and bacteria fractions in the montmorillonite–*B. subtilis* composite as predicted by CA-SCM closely coincided the results obtained from the EXAFS spectra analysis.

Acknowledgements

The study was funded by the National Natural Science Foundation of China (41230854) and project 2662015PY016, 2662015PY116 by the Fundamental Research Funds for the Central Universities. We are also grateful to the beamline BL14W1, Shanghai Synchrotron Radiation Facility for providing the beam time.

References

Akafia, M. M., Reich, T. J. and Koretsky, C. M.: Assessing Cd, Co, Cu, Ni, and Pb sorption on montmorillonite using surface complexation models. Appl. Geochem., 26, 154–157, 2011.

Alessi, D. S. and Fein, J. B.: Cadmium adsorption to mixtures of soil components: Testing the component additivity approach. Chem. Geol., 270, 186–195, 2010.

Angove, M. J., Johnson, B. B. and Wells, J. D.: Adsorption of cadmium(II) on kaolinite. Colloid Surface. A, 126, 137–147, 1997.

Benedicto, A., Degueldre, C. and Missana, T.: Gallium sorption on montmorillonite and illite colloids: Experimental study and modelling by ionic exchange and

surface complexation. Appl. Geochem., 40, 43–50, 2014.

Borrok, D. M. and Fein, J. B.: The impact of ionic strength on the adsorption of protons, Pb, Cd, and Sr onto the surfaces of Gram negative bacteria: testing non-electrostatic, diffuse, and triple-layer models. J. Colloid Interface Sci., 286, 110–126, 2005.

Borrok, D., Fein, J. B. and Kulpa, C. F.: Proton and Cd adsorption onto natural bacterial consortia: Testing universal adsorption behavior. Geochim. Cosmochim. Ac., 68, 3231–3238, 2004.

Bradbury, M. H., Baeyens, B., Geckeis, H. and Rabung, T.: Sorption of Eu(III)/Cm(III) on Ca-montmorillonite and Na-illite. Part 2: Surface complexation modelling. Geochim. Cosmochim. Ac., 69, 5403–5412, 2005.

Christl, I., Milne, C. J., Kinniburgh, D. G. and Kretzschmar, R.: Relating ion binding by fulvic and humic acids to chemical composition and molecular size. 2. metal binding. Environ. Sci. Technol., 35, 2512–2517, 2001.

Chu, Z., Liu, W., Tang, H., Qian, T., Li, S., Li, Z. and Wu, G.: Surface acid-base behaviors of Chinese loess. J. Colloid Interface Sci., 252, 426–32, 2002.

Daughney, C. J., Fowle, D. A. and Fortin, D.: The effect of growth phase on proton and metal adsorption by *Bacillus subtilis*. Geochim. Cosmochim. Ac., 65, 1025–1035, 2001.

Dong, W. and Wan, J.: Additive surface complexation modeling of uranium(VI) adsorption onto quartz-sand dominated sediments. Environ. Sci. Technol., 48,

6569–77, 2014.

Du, H., Chen, W., Cai, P., Rong, X., Dai, K., Peacock, C. L. and Huang, Q.: Cd(II) sorption on montmorillonite-humic acid-bacteria composites. Sci. Rep., 6, 19499, 2016.

Du, Q., Sun, Z. X., Forsling, W. and Tang, H. X.: Acid–base properties of aqueous illite surfaces. J. Colloid Interface Sci., 187, 221–231, 1997.

Fein, J. B., Fowle, D. A., Daughney, C. J., Yee, N. and Davis, T. A.: A chemical equilibrium model for metal adsorption onto bacterial surfaces. Geochim. Cosmochim. Ac., 61, 3319–3328, 1997.

Fein, J. B., Boily, J. F. and Yee, N.: Gorman-Lewis, D.; Turner, B. F., Potentiometric titrations of *Bacillus subtilis* cells to low pH and a comparison of modeling approaches. Geochim. Cosmochim. Ac., 69, 1123–1132, 2005.

Fomina, M. and Gadd, G. M.: Biosorption: current perspectives on concept, definition and application. Bioresour. Technol., 160, 3–14, 2014.

Fowle, D. A. and Fein, J. B.: Competitive adsorption of metal cations onto two gram positive bacteria: Testing the chemical equilibrium model. Geochim. Cosmochim. Ac., 63, 3059–3067, 1999.

Gustafsson, J. P., Persson, I., Oromieh, A. G., van Schaik, J. W., Sjostedt, C. and Kleja, D. B.: Chromium(III) complexation to natural organic matter: mechanisms and modeling. Environ. Sci. Technol., 48, 1753–61, 2014.

He, J. and Chen, J. P.: A comprehensive review on biosorption of heavy metals by

algal biomass: materials, performances, chemistry, and modeling simulation tools. Bioresour. Technol., 160, 67–78, 2014.

Herbelin, A. L. and Westall, J. C.: FITEQL:a computer program for the determination of chemical equilibrium constants from experimental data. Report. 94-01. Department of Chem, Oregon State University, Corvallis, 1999.

Hohl, H. and Stumm, W.: Interaction of Pb^{2+} with hydrous γ - Al_2O_3. J. Colloid Interface Sci., 55, 281–288, 1976.

Hong, Z., Chen,W., Rong, X., Cai, P., Dai, K. and Huang, Q.: The effect of extracellular polymeric substances on the adhesion of bacteria to clay minerals and goethite. Chem. Geol., 360-361, 118–125, 2013.

Hong, Z., Rong, X., Cai, P., Dai, K., Liang, W., Chen, W. and Huang, Q.: Initial adhesion of *Bacillus subtilis* on soil minerals as related to their surface properties. Eur. J. Soil. Sci., 63, 457–466, 2012.

Ikhsan, J., Wells, J. D., Johnson, B. B. and Angove, M. J.: Surface complexation modeling of the sorption of Zn(II) by montmorillonite. Colloid Surface. A, 252, 33–41, 2005.

Kenney, J. P. and Fein, J. B.: Cell wall reactivity of acidophilic and alkaliphilic bacteria determined by potentiometric titrations and Cd adsorption experiments. Environ. Sci. Technol., 45, 4446–4452, 2011.

Kim, S. S., Min, J. H., Lee, J. K., Baik, M. H., Choi J. W. and Shin, H. S.: Effects of pH and anions on the sorption of selenium ions onto magnetite. J. Environ.

547 Radioact., 104, 1–6, 2012.
548 Koopal, L. K., Saito, T., Pinheiro, J. P. and van Riemsdijk, W. H.: Ion binding to
549 natural organic matter: General considerations and the NICA–Donnan model.
550 Colloid Surface. A, 265, 40–54, 2005.
551 Lackovic, K., Angove, M. J., Wells, J. D. and Johnson, B. B.: Modeling the
552 adsorption of Cd(II) onto goethite in the presence of citric acid. J. Colloid
553 Interface Sci., 269, 37–45, 2004a.
554 Lackovic, K., Wells, J. D., Johnson, B. B. and Angove, M. J.: Modeling the
555 adsorption of Cd(II) onto kaolinite and Muloorina illite in the presence of citric
556 acid. J. Colloid Interface Sci., 270, 86–93, 2004b.
557 Landry, C. J., Koretsky, C. M., Lund, T. J., Schaller, M. and Das, S.: Surface
558 complexation modeling of Co(II) adsorption on mixtures of hydrous ferric oxide,
559 quartz and kaolinite. Geochim. Cosmochim. Ac., 73, 3723–3737, 2009.
560 Liu, R. X., Song, Y. H. and Tang, H. X.: Application of the surface complexation
561 model to the biosorption of Cu(II). Adsorpt. Sci. Technol., 31, 1–16, 2013.
562 Liu, W. X., Sun, Z. X., Forsling, W., Du, Q. and Tang, H. X.: A comparative study of
563 surface acid-base characteristics of natural illites from different origins. J. Colloid
564 Interface Sci., 219, 48–61, 1999.
565 Milne, C. J., Kinniburgh, D. G., van Riemsdijk, W. H. and Tipping, E.: Generic
566 NICA-Donnan model parameters for metal-ion binding by humic substances.
567 Environ. Sci. Technol., 37, 958–971, 2003.

568 Moon, E. M. and Peacock, C. L.: Adsorption of Cu(II) to *Bacillus subtilis*: A
569 pH-dependent EXAFS and thermodynamic modelling study. Geochim.
570 Cosmochim. Ac., 75, 6705–6719, 2011.
571 Moon, E. M. and Peacock, C. L.: Adsorption of Cu(II) to ferrihydrite and
572 ferrihydrite–bacteria composites: Importance of the carboxyl group for Cu
573 mobility in natural environments. Geochim. Cosmochim. Ac., 92, 203–219, 2012.
574 Moon, E. M. and Peacock, C. L.: Modelling Cu(II) adsorption to ferrihydrite and
575 ferrihydrite–bacteria composites: Deviation from additive adsorption in the
576 composite sorption system. Geochim. Cosmochim. Ac., 104, 148–164, 2013.
577 Ravel, B. and Newville, M.: ATHENA, ARTEMIS, HEPHAESTUS: data analysis for
578 X-ray absorption spectroscopy using IFEFFIT. J. Synchrotron Radiat., 12,
579 537–541, 2005.
580 Reich, T. J., Das S., Koretsky, C. M., Lund, T. J. and Landry, C. J.: Surface
581 complexation modeling of Pb(II) adsorption on mixtures of hydrous ferric oxide,
582 quartz and kaolinite. Chem. Geol., 275, 262–271, 2010.
583 Schaller, M. S., Koretsky, C. M., Lund, T. J. and Landry, C. J.: Surface complexation
584 modeling of Cd(II) adsorption on mixtures of hydrous ferric oxide, quartz and
585 kaolinite. J. Colloid Interface Sci., 339, 302–9, 2009.
586 Soltermann, D., Baeyens, B., Bradbury, M. H. and Fernandes, M. M.: Fe(II) uptake on
587 natural montmorillonites. II. surface complexation modeling. Environ. Sci.
588 Technol., 48, 8698–705, 2014.

589 Song, Y. T., Swedlund, P., Singha, N. and Swift, S.: Cadmium(II) speciation in
590 complex aquatic systems: A study with ferrihydrite, bacteria, and an organic
591 Ligand. Environ. Sci. Technol., 43, 7430–7436, 2009.
592 Templeton, A. S., Spormann, A. M. and Brown, G. E.: Speciation of Pb(II) Sorbed by
593 *Burkholderia cepacia*/Goethite Composites. Environ. Sci. Technol., 37,
594 2166–2172, 2003.
595 Tertre, E., Castet, S., Berger, G., Loubet, M. and Giffaut, E.: Surface chemistry of
596 kaolinite and Na-montmorillonite in aqueous electrolyte solutions at 25 and 60 ℃:
597 Experimental and modeling study. Geochim. Cosmochim. Ac., 70, 4579–4599,
598 2006.
599 Tournassat, C., Neaman, A., Villieras, F., Bosbach, D. and Charlet, L.:
600 Nanomorphology of montmorillonite particles: Estimation of the clay edge
601 sorption site density by low-pressure gas adsorption and AFM observations. Am.
602 Mineral., 88, 1989–1995, 2003.
603 Wang, Z. and Giammar, D. E.: Mass action expressions for bidentate adsorption in
604 surface complexation modeling: theory and practice. Environ. Sci. Technol., 47,
605 3982–96, 2013.
606 Wang, Z., Lee, S. W., Catalano, J. G., Lezama-Pacheco, J. S., Bargar, J. R., Tebo, B.
607 M. and Giammar, D. E.: Adsorption of uranium(VI) to manganese oxides: X-ray
608 absorption spectroscopy and surface complexation modeling. Environ. Sci.
609 Technol., 47, 850–858, 2013.

610 Weng, L. P., Van Riemsdijk, W. H. and Hiemstra, T.: Cu^{2+} and Ca^{2+} adsorption to
611 goethite in the presence of fulvic acids. Geochim. Cosmochim. Ac., 72,
612 5857–5870, 2008.
613 Yee, N. and Fein, J. B.: Cd adsorption onto bacterial surfaces: A universal adsorption
614 edge? Geochim. Cosmochim. Ac., 65, 2037–2042, 2001.
615
616

Figure Captions

Figure 1. Zeta potential of montmorillonite, *B. subtilis*, and montmorillonite–*B. subtilis* composite at different pH values.

Figure 2. Adsorption of Cd(II) to montmorillonite, *B. subtilis*, and montmorillonite–*B. subtilis* composite as a function of pH in the presence of 0.01 M $NaNO_3$ (symbols are data points and lines are model fits). The sorbent and initial Cd concentration is 1 g L^{-1} and 10 ppm, respectively.

Figure 3. Speciation diagrams for Cd (II) adsorption onto montmorillonite–*B. subtilis* composite at 28 ℃ in the presence of 0.01 M $NaNO_3$, calculated from the surface complexation models (filled squares represent the experimental adsorption data). Cd(II) :10 ppm, composite: 0.875 g L^{-1} Mont +0.125 g L^{-1} *B. subtilis*.

Figure 4. Distribution of the total adsorbed Cd between montmorillonite and *B. subtilis* fractions in the composite predicted by CA-SCM (symbols are data points, lines are model fits) at 28 ℃ in the presence of 0.01 M $NaNO_3$. Cd(II) :10 ppm, composite : 0.875 g L^{-1} Mont +0.125 g L^{-1} *B. subtilis*.

Figure 5. Normalized Cd K-edge k^3-weighted EXAFS spectra of *B. subtilis* (a), montmorillonite (b) and montmorillonite–*B. subtilis* composite (c) at pH 6. Dotted (blue) line display the best 2-component linear combination fit.

Figure 6. Schematic cartoon illustrating Cd binding on clay-bacteria composite.

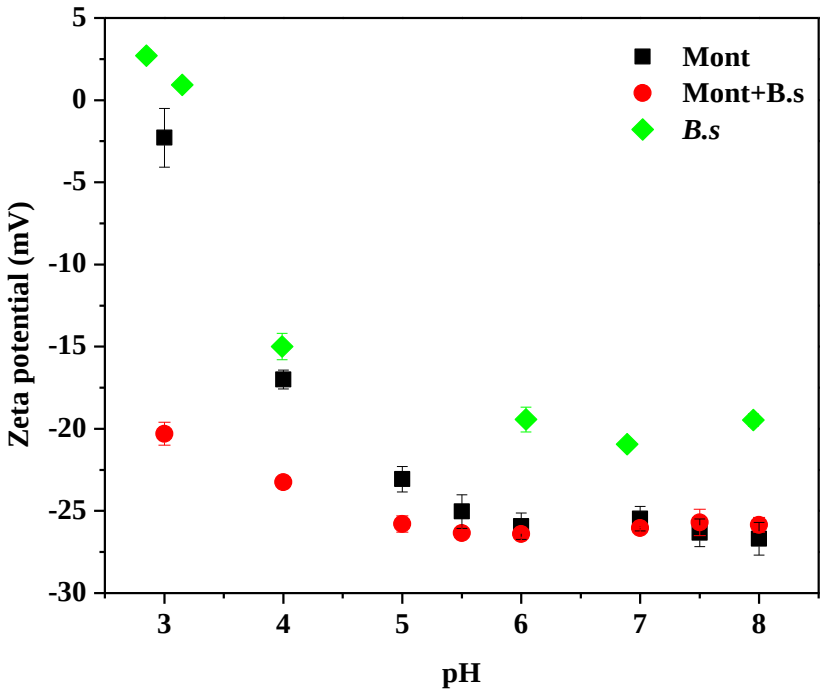

Figure 1. Zeta potential of montmorillonite, *B. subtilis*, and montmorillonite–*B. subtilis* composite at different pH values.

643

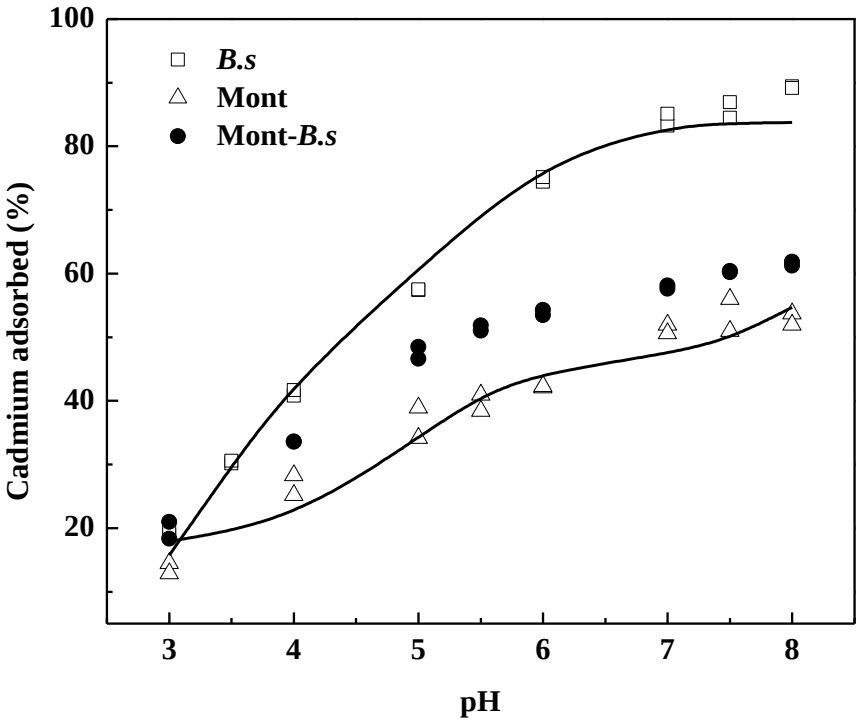

644

645 Figure 2. Adsorption of Cd(II) to montmorillonite, *B. subtilis*, and montmorillonite–*B.*
646 *subtilis* composite as a function of pH in the presence of 0.01 M $NaNO_3$ (symbols are
647 data points and lines are model fits). The sorbent and initial Cd concentration is 1 g
648 L^{-1} and 10 ppm, respectively.

649

650

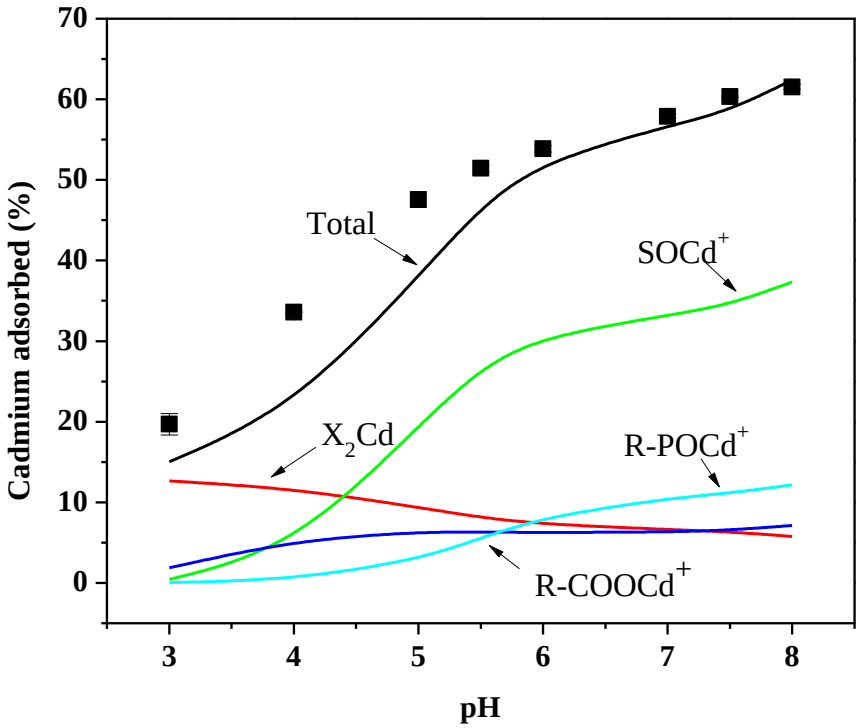

651

652 Figure 3. Speciation diagrams for Cd (II) adsorption onto montmorillonite–*B. subtilis*
653 composite at 28 ℃ in the presence of 0.01 M $NaNO_3$, calculated from the surface
654 complexation models (filled squares represent the experimental adsorption data).
655 Cd(II) :10 ppm, composite: 0.875 g L^{-1} Mont +0.125 g L^{-1} *B. subtilis*.

656

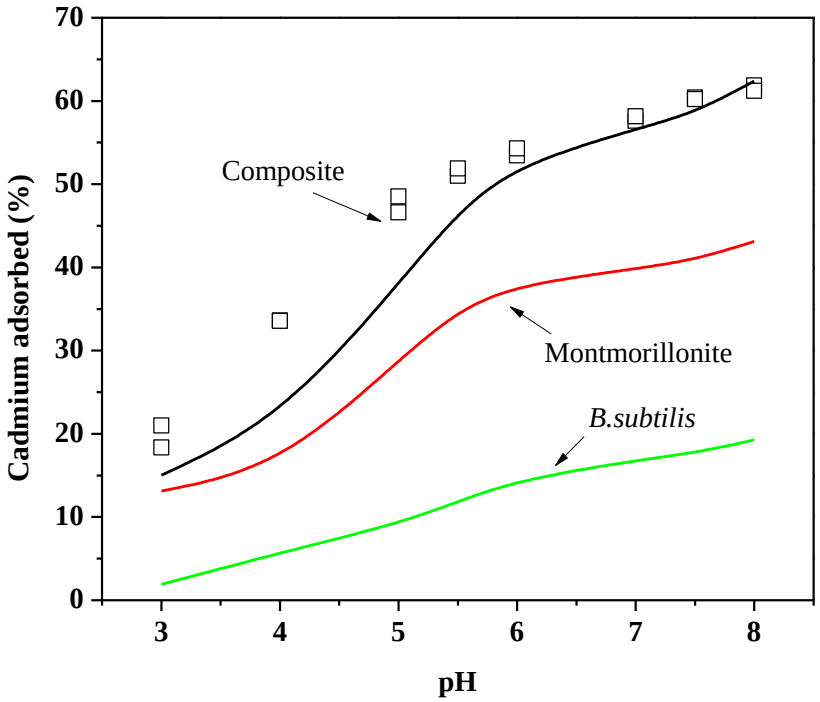

Figure 4. Distribution of the total adsorbed Cd between montmorillonite and *B. subtilis* fractions in the composite predicted by CA-SCM (symbols are data points, lines are model fits) at 28 ℃ in the presence of 0.01 M $NaNO_3$. Cd(II) :10 ppm, composite : 0.875 g L^{-1} Mont +0.125 g L^{-1} *B. subtilis*.

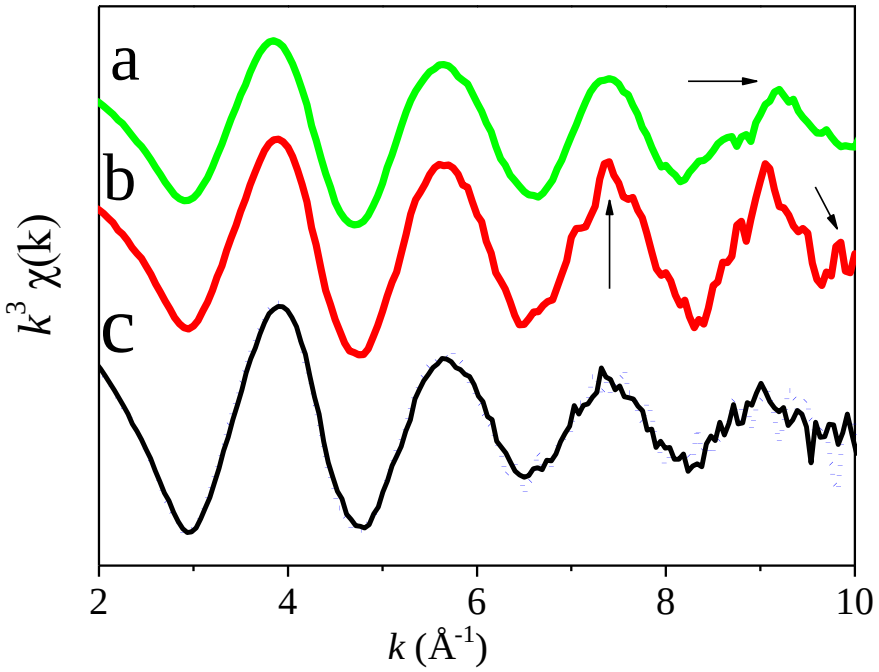

664

665 Fig. 5. Normalized Cd K-edge k^3-weighted EXAFS spectra of *B. subtilis* (a),

666 montmorillonite (b) and montmorillonite–*B. subtilis* composite (c) at pH 6. Dotted

667 (blue) line display the best 2-component linear combination fit.

668

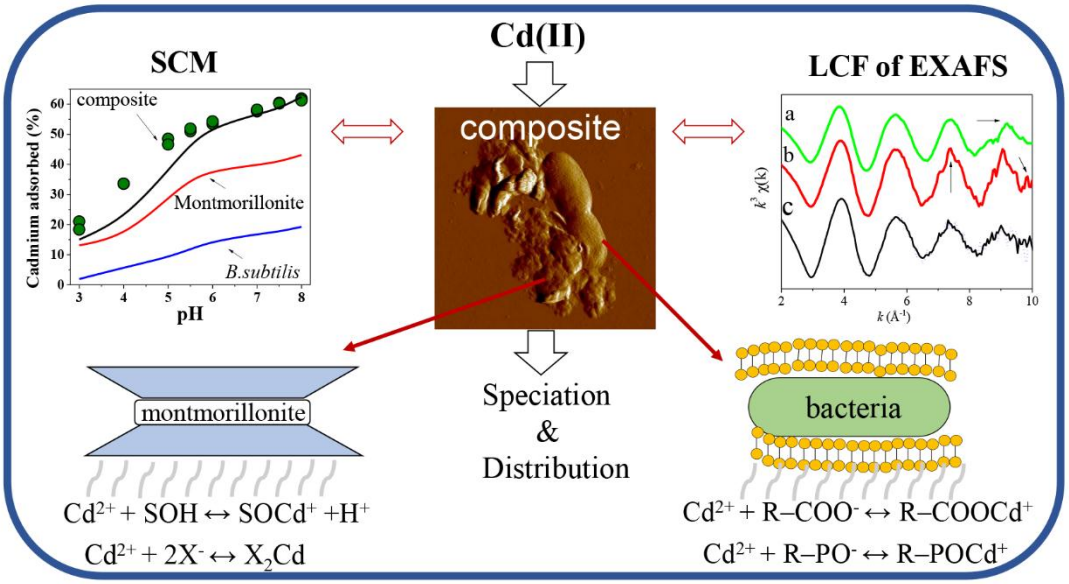

Fig. 6. Schematic cartoon illustrating Cd binding on clay-bacteria composite.

689 Table 1 Surface complexation model parameters for Cd(II) sorption on
690 montmorillonite–*B. subtilis* composite.

Surface area (m^2/g)		422.6 [b]
Total concentration of sites (mmol/g)		
SOH		0.13[b]
WOH		0.50[b]
X^-		0.37[b]
R-COOH		0.09[b]
R-POH		0.07[b]
Specific capacitance (F/m^2)		5.54[b]
Surface reactions		
$LogK_{XH}$	$X^- + H^+ \Leftrightarrow XH$	-2.2[a]
$LogK_{XNa}$	$X^- + Na^+ \Leftrightarrow XNa$	1.4[a]
$LogK_{SO^-}$	$SOH \Leftrightarrow SO^- + H^+$	-4.83 ±0.06[a]
$LogK_{SOH2^+}$	$SOH + H^+ \Leftrightarrow SOH_2^+$	1.86 ±0.06[a]
$LogK_{WO^-}$	$WOH \Leftrightarrow WO^- + H^+$	-8.36 ±0.08[a]
$LogK_{R\text{-}COO^-}$	$R\text{-}COOH \Leftrightarrow R\text{-}COO^- + H^+$	-3.32 ±0.08[a]
$LogK_{R\text{-}PO^-}$	$R\text{-}POH \Leftrightarrow R\text{-}PO^- + H^+$	-5.38 ±0.02[a]
$LogK_{X2Cd}$	$2X^- + Cd^{2+} \Leftrightarrow X_2Cd$	8.30 ±0.04[a]
$LogK_{SOCd^+}$	$SOH + Cd^{2+} \Leftrightarrow SOCd^+ + H^+$	-1.68 ±0.005[a]
$LogK_{R\text{-}COOCd^+}$	$R\text{-}COO^- + Cd^{2+} \Leftrightarrow R\text{-}COOCd^+$	2.54 ±0.005[a]
$LogK_{R\text{-}POCd^+}$	$R\text{-}PO^- + Cd^{2+} \Leftrightarrow R\text{-}POCd^+$	2.87 ±0.02[a]

691 [a] Fixed at those determined for montmorillonite-bacteria composite (obtained from
692 Tables S1 and S2)
693 [b] Calculated using the surface site densities or surface areas or the specific capacitance
694 of the end-member montmorillonite and *B. subtilis* weighted to the mineral:bacteria
695 mass ratio of 7:1.